Solar and solar wind energy drivers for O+ and O2+ ion escape at Mars

Neesha Regmi Schnepf[1], Yaxue Dong[2], David Andrew Brain[2], Kathleen Gwen Hanley[3], William K. Peterson[2], Robert J Strangeway[4], Edward Michael Benjamin Thiemann[5], Jasper S. Halekas[6], Jared Randolph Espley[7], Francis G. Eparvier[5], and James P. Mcfadden[8]

[1]Laboratory for Atmospheric & Space Physics, CU Boulder
[2]University of Colorado Boulder
[3]Space Science Laboratory, UC Berkerley
[4]University of California at Los Angeles
[5]Laboratory for Atmospheric and Space Physics
[6]University of Iowa
[7]NASA Goddard
[8]University of California, Berkeley

July 23, 2023

Abstract

Mars once had a dense atmosphere enabling liquid water existing on its surface, however, much of that atmosphere has since escaped to space. We examine how incoming solar and solar wind energy fluxes drive escape of atomic and molecular oxygen ions (O+ and O2+) at Mars. We use MAVEN data to evaluate ion escape from February 1, 2016 through May 25, 2022. We find that Martian O+, and O2+ all have increased escape flux with increased solar wind kinetic energy flux. Increased solar wind electromagnetic energy flux also corresponds to increased O+ and O2+ escape flux. Increased solar irradiance (both total and ionizing) does not obviously increase escape of O+ and O2+. Together, these results suggest that the solar wind electromagnetic energy flux should be considered along with the kinetic energy flux, and that other parameters should be considered when evaluating solar irradiance's impact on O+ and O2+ escape.

Solar and solar wind energy drivers for O^+ and O_2^+ ion escape at Mars

N. R. Schnepf[1], Y. Dong[1], D. Brain[1], K. G. Hanley[2], W. K. Peterson[1], R. J. Strangeway[3], E. M. B. Thiemann[1], J. S. Halekas[4], J. R. Espley[5], F. Eparvier[1], J. P. McFadden[2]

[1]Laboratory for Atmospheric and Space Physics, University of Colorado Boulder, Boulder, CO, USA
[2]Space Sciences Laboratory, University of California Berkeley, Berkeley, CA, USA
[3]Institute of Geophysics and Planetary Physics, and Department of Earth, Planetary, and Space, University of California Los Angeles, Los Angeles, CA, USA
[4]Department of Physics and Astronomy, University of Iowa, Iowa City, IA, USA
[5]NASA Goddard Space Flight Center, Greenbelt, MD, USA

Key Points:

- Increased solar wind electromagnetic energy flux increases escape of O^+ and O_2^+.
- O^+ and O_2^+ have increased escape rates with increased solar wind kinetic energy.
- Increased solar irradiance does not lead to direct increases of O^+ and O_2^+ escape.

Corresponding author: Neesha R. Schnepf, `neesha.schnepf@lasp.colorado.edu`

Abstract

Mars once had a dense atmosphere enabling liquid water existing on its surface, however, much of that atmosphere has since escaped to space. We examine how incoming solar and solar wind energy fluxes drive escape of atomic and molecular oxygen ions (O^+ and O_2^+) at Mars. We use MAVEN data to evaluate ion escape from February 1, 2016 through May 25, 2022. We find that Martian O^+, and O_2^+ all have increased escape flux with increased solar wind kinetic energy flux. Increased solar wind electromagnetic energy flux also corresponds to increased O^+ and O_2^+ escape flux. Increased solar irradiance (both total and ionizing) does not obviously increase escape of O^+ and O_2^+. Together, these results suggest that the solar wind electromagnetic energy flux should be considered along with the kinetic energy flux, and that other parameters should be considered when evaluating solar irradiance's impact on O^+ and O_2^+ escape.

Plain Language Summary

Mars was once like Earth with a dense atmosphere enabling liquid water to exist on its surface. However, in the billions of years since then, Mars has lost much of its atmosphere to space. We study how energy inputs from the Sun and from the solar wind can drive escape of the ionized constituents of water from Mars' atmosphere. Ion escape is one of several processes of atmospheric loss, and it is a particularly effective process for removing species heavier than hydrogen and helium from terrestrial atmospheres. We find that previously unconsidered energy fluxes may play an important role in driving ion escape.

1 Introduction

Atmospheric escape may be more efficient at Mars than at Earth or Venus, since Mars is the least massive and a weaker gravitation potential leads to a lower escape energy for atmospheric particles. Additionally, without a global magnetic field the solar wind can more directly interact with Mars' atmosphere. This is believed to play a critical role in the escape of planetary ions from Mars' atmosphere. Studying ion escape at Mars is motivated by evidence that early Mars had a dense enough atmosphere to enable liquid water to exist on its surface (Pollack et al., 1987; Jakosky & Phillips, 2001).

Atmospheric ion escape is one of several processes that result in atmospheric loss. Ion escape is a particularly effective process for removing species heavier than hydrogen and helium from terrestrial atmospheres (e.g. D. Brain et al. (2016, 2017); Ramstad and Barabash (2021)). For decades now, there has been much effort towards determining the relationship between Mars' atmospheric ion escape and incoming solar and solar wind conditions (for example, see, Lundin et al. (1989, 1990); Nilsson et al. (2010); Ramstad et al. (2015); Y. Dong et al. (2017); Dubinin, Fraenz, Pätzold, McFadden, Mahaffy, et al. (2017); Dubinin, Fraenz, Pätzold, McFadden, Halekas, et al. (2017); Nilsson et al. (2021); Y. Dong et al. (2022)). Solar wind kinetic energy, in the form of solar wind dynamic pressure, and solar ionizing irradiation (typically determined from extreme ultraviolet observations) are the two most studied incoming energy sources for Martian atmospheric ion escape. While studies have considered upstream solar wind magnetic field strength (e.g. Nilsson et al. (2010)), or local crustal magnetic field strength (e.g. Weber et al. (2021)), no previous study has examined the role of the incoming solar wind electromagnetic field energy flux (i.e. the Poynting flux). Additionally, influences of total solar irradiance variability have mostly been considered in studies of Mars' neutral hydrogen exosphere (e.g. Bhattacharyya et al. (2015); J. Halekas (2017)), but not in studies of escaping ions.

Here, we examine how incoming solar and solar wind energy fluxes drive escape of atomic and molecular oxygen ions (O^+ and O_2^+). Our goal is to determine how the escape of O^+ and O_2^+ ions depends on solar and solar wind energy inputs at Mars. As il-

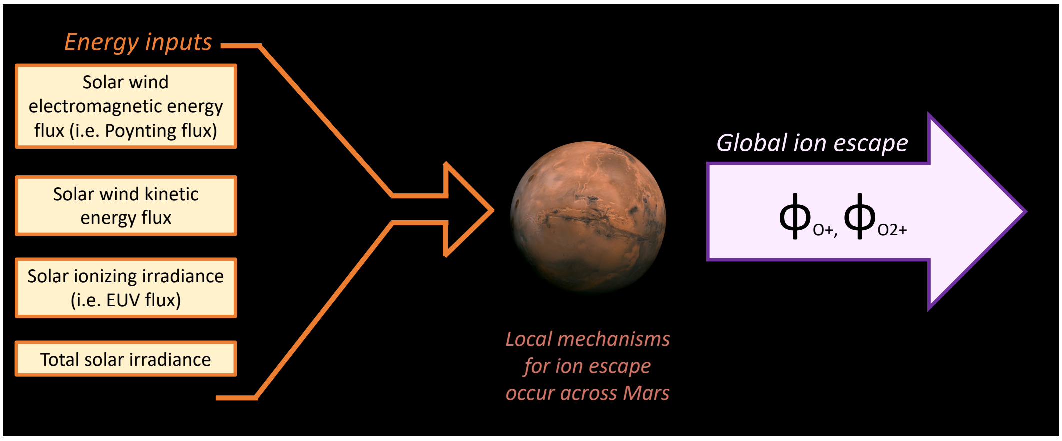

Figure 1. Overview of our study's aim: how does incoming solar and solar wind energy drive global ion escape for O^+ and O_2^+?

lustrated in Figure 1, energy is input to the Mars system from the Sun (i.e. the solar ionizing irradiance and total solar irradiance) and from the solar wind (i.e. the electromagnetic energy flux, also known as the Poynting flux, and the kinetic energy flux). These solar energy inputs drive a multitude of mechanisms local to Mars that lead to ion escape (e.g. plasma waves, electric field forces, collisions, sputtering; for example, see Ergun et al. (2006)). However, our question is global in nature: how do Mars' global ion escape rates depend on each solar and solar wind energy input? By comparing fairly simple incoming solar and solar wind energy fluxes with Mars' global O^+ and O_2^+ flux rates, we aim to provide results that may be easily compared against other planets (e.g. how do O^+/O_2^+ flux rates instead depend on these drivers at Earth, Venus, or an exoplanet?)

2 MAVEN Ion Flux Observations

Data from the Mars Atmosphere and Volatile Evolution (MAVEN) mission's SupraThermal and Thermal Ion Composition (STATIC) instrument were used. STATIC measures the in situ distribution of ions as a function of energy (0.1 eV – 30 keV; dE/E$\sim$15%), mass (1024 bins; 1– $\sim$ 100 AMU), direction (360° × 90° field of view), and time (4s resolution) (McFadden et al., 2015).

Ion flux observations from February 1, 2016 through to May 25, 2022 were selected either from MAVEN STATIC d1 or d0 data. These data products only differ in their temporal resolution: d0 samples data as fast as every 32 seconds, whereas d1 has a sampling resolution reaching down to every 4 seconds. Both of these data products include 32 energy channels and 8 mass channels, as well as 4 polar angles (with 11.1 degrees resolution in each direction) and 16 azimuthal angles (of 22.5 degrees resolution). We prioritized using d1 data and used d0 whenever d1 was unavailable. While MAVEN reached Mars in November 2014, we use STATIC data starting in February 2016 because this is when STATIC data started including key background and directional corrections.

Following the methods of D. A. Brain et al. (2015), we select observations when MAVEN was located within the spherical shell centered on Mars between 1.25 and 1.45 R_M (i.e. an altitude range of 850-1530 km). Our study focuses on O^+ and O_2^+. We limit STATIC data to those species by using specific mass and energy channels. For O^+ and O_2^+, to avoid ion suppression issues (i.e. localized changes in electric potential on the STATIC elelectrostatic analyzer surface that limit STATIC's ability to accurately measure low energy ions, see Fowler et al. (2022) for more details), we use the same energy range ($\geq$6

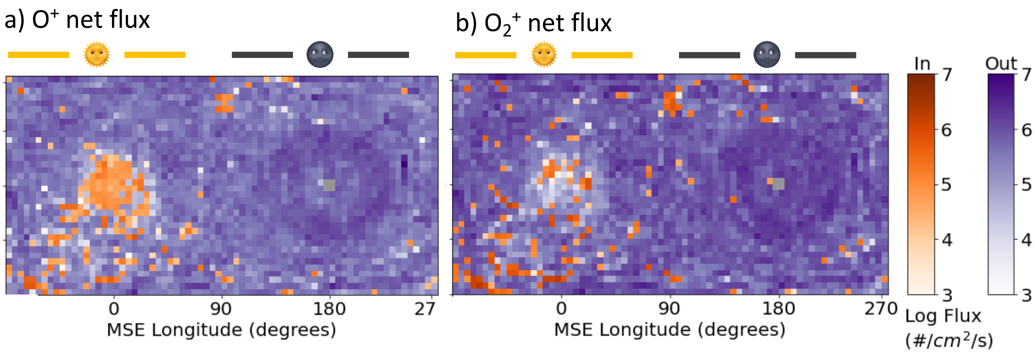

Figure 2. The average observed outwards (purple) and inwards (orange) net flux for O^+ and O_2^+ from February 1, 2016 to May 21, 2022. The data is binned onto a Mars Solar Electric grid; the day- side and night-side of Mars are denoted accordingly.

eV) as Y. Dong et al. (2017). This captures all O^+ and O_2^+ observations above Mars' escape energy.

Of course, STATIC cannot observe the entire distribution of plasma, it is limited in its field of view, and it is difficult for us to correct what may be missing. Thus, we are implicitly assuming that STATIC does see the bulk of the distribution, and that what is missing will not be beyond the standard deviation of what is observed.

The ion fluxes are calculated from observations of ion density and ion velocity. The ion velocity is corrected for spacecraft velocity, as well as for background straggling protons (Hanley, 2023), and for the spacecraft electric potential (Fowler et al., 2022). Ion fluxes are first determined in STATIC instrument coordinates, and then translated from that to Mars Solar Electric (MSE) coordinates. MSE coordinates are defined such that $\hat{x}$ points from Mars to the Sun and $\hat{z}$ is parallel to the solar wind's electric field. The $\hat{y}$ direction then completes the orthogonal system.

We mapped the radial component of all ion flux observations into a $5° \times 5°$ spatial grid on our spherical surface. Figure 2 shows the average observed outwards and inwards ion fluxes for each species across this MSE global grid and across the entire duration of our study. Overall, both O^+ and O_2^+ see their largest inwards signal on the day-side of Mars and their most significant outwards flux is on the night-side.

3 Solar and Solar Wind Energy Fluxes

We determine Mars' incoming solar wind energy fluxes using data from MAVEN's magnetometer (Connerney et al., 2015) and Solar Wind Ion Analyzer (SWIA; J. S. Halekas et al. (2015)). We use these instruments' observations upstream of Mars' bow shock (J. S. Halekas et al., 2017) to calculate the incoming kinetic energy flux and electromagnetic (EM) energy flux. Solar wind kinetic energy flux has mostly been studied in the form of solar wind dynamic pressure (Lundin et al., 2008; Dubinin, Fraenz, Pätzold, McFadden, Halekas, et al., 2017; Ramstad et al., 2018; Dubinin et al., 2021; Nilsson et al., 2021).

We calculate the kinetic energy flux ($\mathbf{K}$) from SWIA's observed solar wind dynamic pressure ($\mathbf{p}$) and solar wind ion velocity ($\mathbf{v}$):

$$|\mathbf{K}| = \frac{1}{2}|\mathbf{p}||\mathbf{v}| \ . \tag{1}$$

Meanwhile, solar wind electromagnetic energy flux can be decomposed into direct current (DC) and alternating current (AC; also known as Alfvén Poytning flux) contributions. Lennartsson et al. (2004) examined the role of incoming solar wind energy on ion escape at Earth, and chose to simply use the DC EM energy flux. The AC Poynting flux is more challenging to calculate since it involves band-pass filtering the upstream data and this data is not collected consistently throughout the mission. This is evident in Figure 3, which shows the time series of solar wind kinetic and EM energy fluxes, as well as the gaps in their observations.

The DC solar wind EM energy flux is given as:

$$\mathbf{S} = \frac{1}{\mu_0}\mathbf{E} \times \mathbf{B}, \tag{2}$$

where μ_0 is the vacuum magnetic permeability, $\mathbf{B}$ is the solar wind magnetic field (measured by MAVEN's magnetometer), and $\mathbf{E}$ is the solar wind electric field. Instead of using direct measurements of $\mathbf{E}$, we use the substitution $\mathbf{E} = -\mathbf{v} \times \mathbf{B}$ to obtain

$$\mathbf{S} = -\frac{1}{\mu_0}(\mathbf{v} \times \mathbf{B}) \times \mathbf{B}. \tag{3}$$

As seen in Figure 3, the solar wind EM energy flux predominantly ranges from 10^{-4} to 10^{-2} mW/m^2, whereas the kinetic energy flux spans 10^{-2} to 1 mW/m^2.

For solar irradiance, we consider both the Sun's ionizing irradiance and the total solar irradiance at Mars. For solar ionizing irradiance, we use MAVEN's extreme ultraviolet monitor (EUVM; Eparvier et al. (2015)) and the Flare Irradiance Spectral Model-Mars (FISM-M; Thiemann et al. (2017)). For each MAVEN orbit, we integrate from 0 to 91 nm to obtain the solar ionizing irradiance for our focus ion species (H^+, O^+, and O_2^+) (Schunk & Nagy, 2009). The time series of ionizing irradiance is depicted in Figure 3 with the orange line.

We also consider the total solar irradiance (TSI) at Mars since non-ionizing irradiance plays an indirect role in ion escape, and ionizing irradiance is a small fraction of the TSI. We obtain Mars' TSI by using the mean value at Earth (1361 W/m^2) (Dudok de Wit et al., 2017), and then using Earth's and Mars' distances from the Sun to calculate the TSI at Mars. The TSI time series is illustrated in Figure 3 with the red line. Note that ionizing irradiance typically exceeds the solar wind energy fluxes, however, it is a fraction of the total solar irradiance.

4 Comparing ion escape to the incoming solar and solar wind energy drivers

All ion flux observations were paired to their nearest-in-time solar and solar wind driver observations. Marquette et al. (2018) showed that solar wind speed and magnetic field stay coherent through the duration of a MAVEN orbit ($\sim$ 4.5 hours). Thus, in our analysis if the nearest-in-time upstream observation exceeded a time difference of 4.5 hours, the ion flux observation was discarded.

After pairing ion flux observations to upstream energy inputs, for each driver, the ion flux observations were ranked by ascending driver value. Then, the ion flux data were binned such that each bin had an equivalent number of observations. For the solar wind energy fluxes, $\sim$200,000 observations per bin provided adequate data coverage across the planet (see Supplementary Figures S1 and S2) and led to a total of 9 bins of different driver average value. Meanwhile, ranking the data by solar irradiance led to significant biases in the spatial coverage. This is largely because MAVEN's orbit varies with the season and solar irradiance is a seasonal signal. Thus, for ionizing irradiance we needed $\sim$300,000 observations per bin to have coverage equivalent to the solar wind drivers. This led to

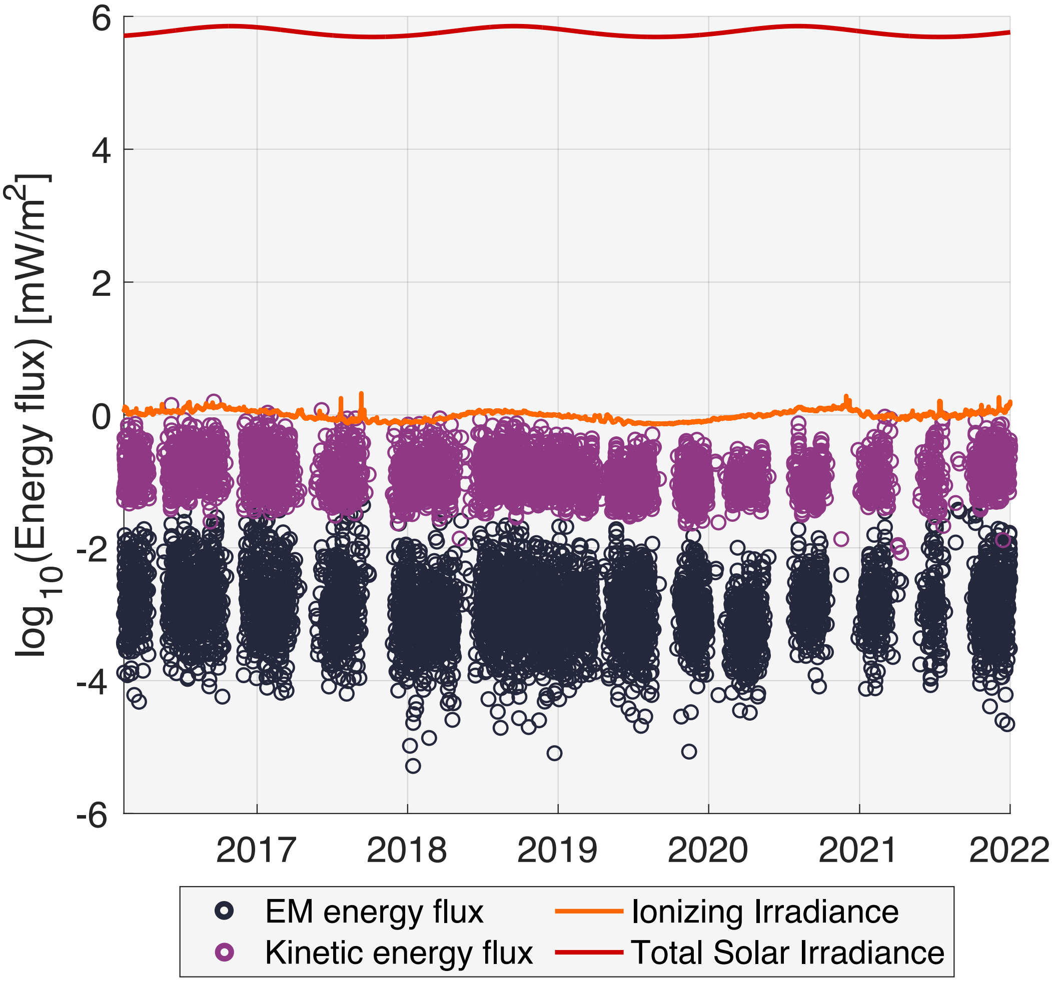

Figure 3. Time series of the considered solar wind and solar energy fluxes. Black circles: solar wind electromagnetic energy flux. Magenta circles: solar wind kinetic energy flux. Orange line: solar ionizing irradiance. Red line: total solar irradiance. Gaps are due to times when MAVEN was not sampling the solar wind.

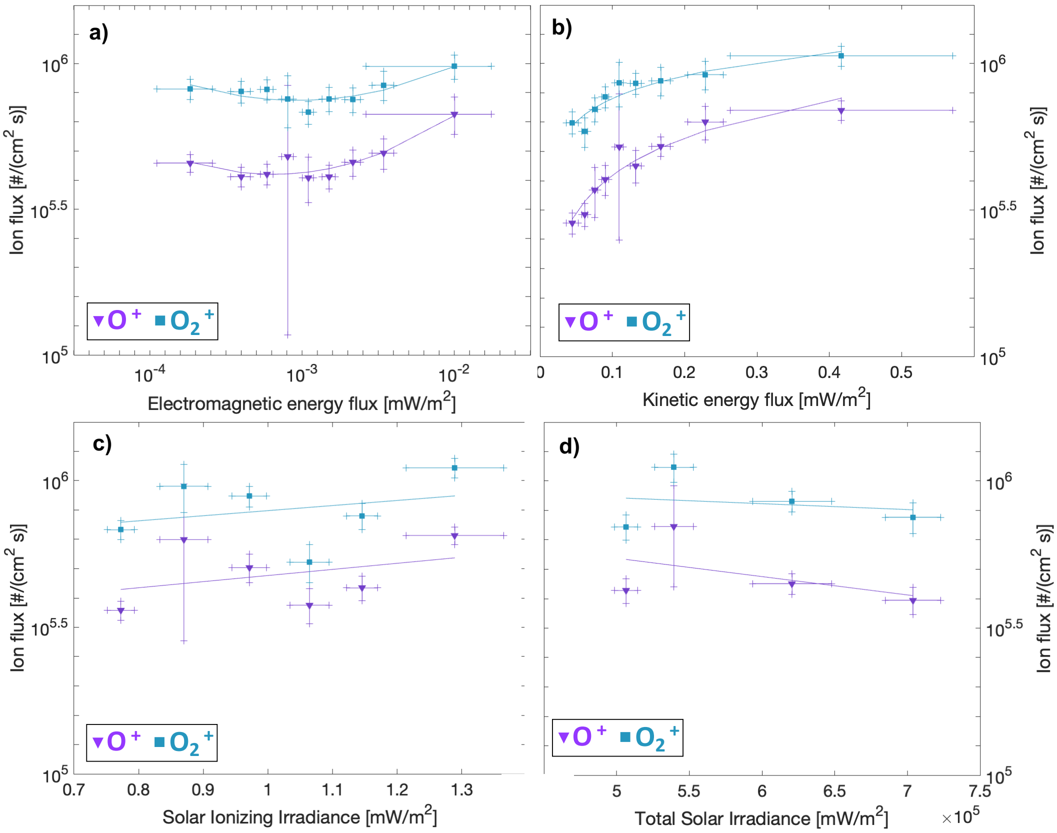

Figure 4. The global net ion flux for each solar and solar wind energy driver and for each ion species (purple triangles: O^+, blue squares: O_2^+). The horizontal whiskers denote the standard deviation of the bin's energy flux values and the vertical whiskers mark the ion flux uncertainty. Solid lines depict the best fit equations shown in Table 1. The top row shows ion flux versus a) solar wind electromagnetic energy flux and b) solar wind kinetic energy flux. The next row shows ion flux versus c) solar ionizing irradiance and (d) total solar irradiance.

6 bins (Supplementary Figure S3 shows the spatial coverage and data density for the ionizing irradiance bins). For TSI, the spatial bias was more extreme and ∼500,000 observations per bin were instead needed (leading to only 4 bins of different average TSI; their spatial coverage and data density is shown in Supplementary Figure S4). Table 1 specifies the number of observations included in each driver's bin.

For each energy driver's ion flux bin, we calculated the average global net radial ion flux for each species. Figure 4 shows each bin's global net ion flux for each driver. In each scatter plot, the horizontal whiskers show the standard deviation in the upstream driver's bin values and the vertical whiskers correspond to the uncertainty in the global ion flux average. This uncertainty was calculated using the standard deviation of each grid cell's ion flux observations and propagated to the global average ion flux value.

4.1 Solar Wind Electromagnetic Energy Flux

Figure 4a shows global ion flux versus solar wind EM energy flux. The oxygen ion species (O^+: purple triangles, O_2^+: blue squares) both have increased ion escape with increased solar wind DC EM energy flux, with a general trend best described using a quadratic equation. Table 1 shows the best fit equation illustrated in the figure, as well as its fairly strong r^2 correlation value.

The rightmost bin has the largest EM energy flux variance since it is sampling the more extreme EM flux values. Future studies should be able to incorporate additional data during the solar cycle maximum to improve the sampling in the most extreme bin.

The role of solar wind EM flux in ion escape at Mars has not been considered in previous studies. However, this energy source should be considered as a possibly important driver of O^+ and O_2^+ escape. Solar wind energy can be transferred to ions through collisions, or through electromagnetic fields. Even though Figure 3 shows that the solar wind EM energy flux is smaller in amplitude than the kinetic energy flux, EM fields may be a more efficient method of transferring energy from the solar wind to ions. Future studies could better constrain ion escape's dependency on this driver by utilizing longer time-series of data, as well as performing modelling work to determine what physical processes may be causing the observed dependency on solar wind EM flux for ion escape. Additionally, because there is some mutual correlation between the solar wind's EM energy flux and kinetic energy flux (see Supplementary Figure S9) due to both parameters depending on solar wind velocity, future studies should consider examining ion flux's dependency on solar wind density, velocity, and interplanetary magnetic field simultaneously.

4.2 Solar Wind Kinetic Energy Flux

Figure 4b shows global ion flux versus solar wind kinetic energy flux. Similar to the solar wind EM energy flux, the rightmost bin has the largest horizontal whiskers because it is sampling the more extreme solar wind kinetic energy conditions and has the largest standard deviation.

All three species show an increase in outwards ion flux with an increase in solar wind kinetic energy. This matches well with some previous studies (Lundin et al., 2008; Dubinin, Fraenz, Pätzold, McFadden, Halekas, et al., 2017; Dubinin et al., 2021) examining Martian ion escape's dependence on solar wind dynamic pressure (which relates to kinetic energy flux as shown in equation 1). However, there are some studies which found the opposite trend (Ramstad et al., 2018; Nilsson et al., 2021): that ion escape decreases with increasing solar wind dynamic pressure (or increasing kinetic energy flux). These two studies both evaluated solar wind dynamic pressure simultaneously with the solar ionizing irradiance. Like the first set of studies, we do not simultaneously fit for both solar wind kinetic energy and solar ionizing irradiance. Indeed, as shown in Supplementary Figures 10-13, solar wind energy fluxes do not seem correlated to solar ionizing irradiance (nor do they seem correlated to TSI). Thus, we decided a simultaneous fit of multiple (ideally, of all four) energy drivers was beyond the scope of this study.

MAVEN is starting to collect data from the current solar maximum. Future studies should utilize data from more of the solar cycle maximum so the extreme-most bin can be separated into multiple bins of higher solar wind kinetic energy flux. Such future studies will be able to answer the question: will the ion escape continue to increase as solar wind kinetic energy flux increases?

4.3 Solar Ionizing Irradiance

Figure 4c shows global ion flux versus solar ionizing irradiance. As described in Section 3, the solar ionizing irradiance is predominantly extreme ultraviolet (EUV) spectra (Thiemann et al., 2017; Eparvier et al., 2015). The binning differs from the solar wind energy fluxes; bins now use over 300,000 observations, yielding six bins rather than nine.

We find that increasing the solar ionizing irradiance imperceptibly changes the ion flux for O^+ and O_2^+. Indeed, Table 1 shows these species results had a best-fit line with a slight positive slope but very weak correlation. This differs from the results of Y. Dong et al. (2017) and Y. Dong et al. (2022). However, those studies have a couple major differences with this study: 1) they constrained ionizing irradiance's influence on ion escape while controlling for other variations in solar wind conditions and 2) they utilized an earlier time period of data which included larger amplitudes of solar ionizing irradiance. We did not also use that earlier data because of known issues with the STATIC ion directions for that time period (Fowler et al., 2022; Hanley, 2023). We hope that future studies will be able to take advantage of the next solar maximum so that a wider range of solar ionizing irradiance can be compared to ion fluxes. We also encourage future work to perform a fit of all solar and solar wind drivers simultaneously.

Our results are instead comparable to studies which simply evaluate the influence of solar ionizing irradiance on O^+ and O_2^+ at altitudes similar to our study (Dubinin, Fraenz, Pätzold, McFadden, Mahaffy, et al., 2017; Dubinin, Fraenz, Pätzold, McFadden, Halekas, et al., 2017). The lack of a relationship between ionizing irradiance and oxygen ion fluxes suggests that the increase in oxygen ions within Mars' ionosphere is not translating to increased outwards flux. Indeed, modelling studies show Mars' oxygen ions have mixed dependency on ionizing irradiance for escape; whether a study finds increased or decreased O^+/O_2^+ escape with ionizing irradiance depends on what other parameters the study considers (C. Dong et al., 2015; Brecht et al., 2016; Cravens et al., 2017). As Brecht et al. (2016) states, the system is very nonlinear.

4.4 Total Solar Irradiance

Figure 4f shows global ion flux versus total solar irradiance (TSI). The binning differs from the other energy fluxes; bins now use 488,822 ion flux observations, yielding four bins rather than six or nine. Even with so few bins, some patterns emerge.

O^+ has large ion flux uncertainty in the second bin, suggesting that O^+'s escape flux stays fairly flat with increased TSI. Like O^+, O_2^+ also has a weakly correlated, flat dependency on TSI. Future studies might investigate whether other Martian seasonal parameters should be constrained when examining ion escape's dependency on TSI.

5 Conclusions and Outlook

We evaluate solar and solar wind energy drivers for atomic and molecular oxygen ions (O^+ and O_2^+). As shown in Figure 1, our analysis includes both solar wind kinetic energy (considered in dynamic pressure form in several previous studies) and electromagnetic energy (unconsidered in previous studies). We find that as both of these solar wind energy fluxes increase, there is increased outwards flux of O^+/O_2^+.

Along with considering these solar wind energy fluxes, we also evaluate both the much studied solar ionizing irradiance and the less considered total solar irradiance. We find that the escape fluxes of O^+/O_2^+ lack a clear relationship with both types of solar irradiance.

We strongly encourage future studies determining empirical relationships between Martian O^+/O_2^+ ion escape and solar drivers to simultaneously consider all of the solar and solar wind energy sources considered here. Further modelling work exploring the possible processes at play for each of these ion species and each of these drivers would also be helpful to understand the underlying physics of the different regimes we observe. And finally, we encourage comparisons to be made examining ion escape's dependency on these solar and solar wind drivers at other planets both within, and beyond, our solar system.

Table 1. Comparing ion escape for O^+ and O_2^+ to incoming solar and solar wind energy fluxes. For each incoming energy flux, the number of observations per bin, the best fit equation, and the r^2 correlation coefficient are given.

	Solar Wind Electromagnetic Energy Flux		
	# obs per bin	Best fit equation	r^2
O^+	217254	$O^+(x) = 0.14x^2 + 0.90x + 7.0$	0.87
O_2^+	217254	$O_2^+(x) = 0.11x^2 + 0.66x + 6.9$	0.75
	Solar Wind Kinetic Energy Flux		
	# obs per bin	Best fit equation	r^2
O^+	217254	$O^+(x) = 6.0 + 0.18 \log x$	0.92
O_2^+	217254	$O_2^+(x) = 6.1 + 0.11 \log x$	0.88
	Solar Ionizing Irradiance		
	# obs per bin	Best fit equation	r^2
O^+	325882	$O^+(x) = 0.07x + 5.6$	0.13
O_2^+	325882	$O_2^+(x) = 0.05x + 5.8$	0.08
	Total Solar Irradiance		
	# obs per bin	Best fit equation	r^2
O^+	488822	$O^+(x) = -6.2 \times 10^{-7}x + 6.0$	0.24
O_2^+	488822	$O_2^+(x) = -2.0 \times 10^{-7}x + 6.0$	0.04

6 Data Availability Statement

MAVEN L2 STATIC data used to create the H^+, O^+, and O_2^+ fluxes are publicly available at NASA's Planetary Data System (`https://pds-ppi.igpp.ucla.edu/search/view/?f=yes&id=pds://PPI/maven.static.c`). MAVEN EUVM data used here to calculate the total solar irradiance and total ionizing solar irradiance are also publicly available at NASA's Planetary Data System (`https://pds-ppi.igpp.ucla.edu/search/view/?f=yes&id=pds://PPI/maven.euv.modelled`). The upstream solar wind data used to obtain solar wind electromagnetic and kinetic energy fluxes are publicly available through the University of Iowa (`http://homepage.physics.uiowa.edu/~jhalekas/drivers.html`).

Acknowledgments

This work was supported by the NASA MAVEN project through the Mars Exploration Program.

References

Bhattacharyya, D., Clarke, J. T., Bertaux, J.-L., Chaufray, J.-Y., & Mayyasi, M. (2015). A strong seasonal dependence in the martian hydrogen exosphere. *Geophysical Research Letters*, *42*(20), 8678–8685.

Brain, D., Bagenal, F., Ma, Y.-J., Nilsson, H., & Stenberg Wieser, G. (2016). Atmospheric escape from unmagnetized bodies. *Journal of Geophysical Research: Planets*, *121*(12), 2364–2385.

Brain, D., Barabash, S., Bougher, S., Duru, F., Jakosky, B., & Modolo, R. (2017). Solar wind interaction and atmospheric escape. In *The Atmosphere and Climate of Mars* (pp. 464–496). Cambridge: Cambridge University Press.

Brain, D. A., McFadden, J. P., Halekas, J. S., Connerney, J. E. P., Bougher, S. W., Curry, S., ... Seki, K. (2015). The spatial distribution of planetary ion fluxes near mars observed by maven. *Geophysical Research Letters*, *42*, 9142–9148. doi: 10.1002/2015GL065293.

Brecht, S. H., Ledvina, S. A., & Bougher, S. W. (2016). Ionospheric loss from mars as predicted by hybrid particle simulations. *Journal of Geophysical Research: Space Physics*, *121*(10), 10–190.

Connerney, J. E. P., Espley, J., Lawton, P., Murphy, S., Odom, J., Oliversen, R., & Sheppard, D. (2015). The maven magnetic field investigation. *Space Science Reviews*, *195*(1-4), 257–291. doi: 10.1007/s11214-015-0169-4

Cravens, T. E., Hamil, O., Houston, S., Bougher, S., Ma, Y., Brain, D., & Ledvina, S. (2017). Estimates of ionospheric transport and ion loss at mars. *Journal of Geophysical Research: Space Physics*, *122*(10), 10–626.

Dong, C., Bougher, S. W., Ma, Y., Toth, G., Lee, Y., Nagy, A. F., ... Najib, D. (2015). Solar wind interaction with the martian upper atmosphere: Crustal field orientation, solar cycle, and seasonal variations. *Journal of Geophysical Research: Space Physics*, *120*(9), 7857–7872.

Dong, Y., Brain, D., Ramstad, R., Fang, X., McFadden, J., Halekas, J., ... Jakosky, B. (2022). The dependence of martian ion escape on solar euv irradiance as observed by maven. *Icarus*, 115288. doi: 10.1016/j.icarus.2022.115288

Dong, Y., Fang, X., Brain, D. A., McFadden, J. P., Halekas, J. S., Connerney, J. E. P., ... Jakosky, B. M. (2017). Seasonal variability of martian ion escape through the plume and tail from maven observations. *Journal of Geophysical Research: Space Physics*, *122*, 4009-4022. doi: 10.1002/2016JA023517

Dubinin, E., Fraenz, M., Pätzold, M., McFadden, J., Halekas, J. S., DiBraccio, G. A., ... Zelenyi, L. (2017). The effect of solar wind variations on the escape of oxygen ions from mars through different channels: Maven observations. *Journal of Geophysical Research: Space Physics*, *122*, 11,285–11,301. doi: 10.1002/2017JA024126

Dubinin, E., Fraenz, M., Pätzold, M., McFadden, J., Mahaffy, P. R., Eparvier, F., ... Zelenyi, L. (2017). Effects of solar irradiance on the upper ionosphere and oxygen ion escape at mars: Maven observations. *Journal of Geophysical Research: Space Physics*, *122*, 7142–7152. doi: 10.1002/2017JA024126

Dubinin, E., Fraenz, M., Pätzold, M., Tellman, S., Woch, J., McFadden, J., & Zelenyi, L. (2021). Bursty ion escape fluxes at mars. *Journal of Geophysical Research: Space Physics*, *126*, e2020JA028920. doi: 10.1029/2020JA028920

Dudok de Wit, T., Kopp, G., Fröhlich, C., & Schöll, M. (2017). Methodology to create a new total solar irradiance record: Making a composite out of multiple data records. *Geophysical Research Letters*, *44*, 1196–1203. doi: 10.1002/2016GL071866

Eparvier, F. G., Chamberlin, P. C., Woods, T. N., & Thiemann, E. M. B. (2015). The solar extreme ultraviolet monitor for maven. *Space Science Reviews*, *195*, 293–301. doi: 10.1007/s11214-015-0195-2

Ergun, R. E., Andersson, L., Peterson, W. K., Brain, D., Delory, G. T., Mitchell, D. L., ... Yau, A. W. (2006). Role of plasma waves in mars' atmospheric loss. *Geophysical Research Letters*, *33*, L14103. doi: 10.1029/2006GL025785

Fowler, C., McFadden, J., Hanley, K., Mitchell, D., Curry, S., & Jakosky, B. (2022). In-situ measurements of ion density in the martian ionosphere: Underlying structure and variability observed by the maven-static instrument. *Journal of Geophysical Research: Space Physics*, *127*(8), e2022JA030352.

Halekas, J. (2017). Seasonal variability of the hydrogen exosphere of mars. *Journal of Geophysical Research: Planets*, *122*(5), 901–911.

Halekas, J. S., Ruhunusiri, S., Harada, Y., Collinson, G., Mitchell, D. L., Mazelle, C., ... Jakosky, B. M. (2017). Structure, dynamics, and seasonal variability of the mars-solar wind interaction: Maven solar wind ion analyzer in-flight performance and science results. *Journal of Geophysical Research: Space Physics*, *122*(1), 547–578. doi: 10.1002/2016JA023167

Halekas, J. S., Taylor, E. R., Dalton, G., Johnson, G., Curtis, D. W., McFadden, J. P., ... Jakosky, B. M. (2015). The Solar Wind Ion Analyzer for MAVEN. *Space Science Reviews*, *195*(1-4), 125–151. doi: 10.1007/s11214-013-0029-z

Hanley, K. G. (2023). *The beginnings of cold ion outflow at mars: Supply and energization near the exobase* (Unpublished doctoral dissertation). University of California, Berkeley.

Jakosky, B. M., & Phillips, R. J. (2001). Mars' volatile and climate history. *Nature*, *412*(6843), 237–244.

Lennartsson, O. W., Collin, H. L., & Peterson, W. K. (2004). Solar wind control of earth's h^+ and o^+ outflow rates in the 15-ev to 33-kev energy range. *Journal of Geophysical Research*, *109*(A12212). doi: 10.1029/2004JA010690

Lundin, R., Barabash, S., Fedorov, A., Holmström, M., Nilsson, H., & Sauvaud, J.-A. (2008). Solar forcing and planetary ion escape from mars. *Geophysical Research Letters*, *35*, L09203. doi: 10.1029/2007GL032884

Lundin, R., Zakharov, A., Pellinen, R., Barabash, S. W., Borg, H., Dubinin, E. M., ... N., P. (1990). Aspera/phobos measurements of the ion outflow from the martian ionosphere. *Geophysical Research Letters*, *17*, 873-876. doi: 10.1029/GL017i006p00873

Lundin, R., Zakharov, A., Pellinen, R., Borg, H., Hultqvist, B., N., P., ... Koskinen, H. (1989). First measurements of the ionospheric plasma escape from mars. *Nature*, *341*(6243), 609-612. doi: 10.1038/341609a0

Marquette, M. L., Lillis, R. J., Halekas, J. S., Luhmann, J. G., Gruesbeck, J. R., & Espley, J. R. (2018). Autocorrelation study of solar wind plasma and imf properties as measured by the maven spacecraft. *Journal of Geophysical Research: Space Physics*, *123*(4), 2493–2512.

McFadden, J. P., Kortmann, O., Curtis, D., Dalton, G., Johnson, G., Abiad, R., ... Jakosky, B. (2015). Maven suprathermal and thermal ion compostion (static) instrument. *Space Science Reviews*, *195*(1-4), 199–256. doi: 10.1007/s11214-015-0175-6

Nilsson, H., Carlsson, E., Brain, D. A., Yamauchi, M., Holmström, M., Barabash, S., . . . Futaana, Y. (2010). Ion escape from mars as a function of solar wind conditions: A statistical study. *Icarus*, 40–49. doi: 10.1016/j.icarus.2009.03.006

Nilsson, H., Zhang, Q., Wieser, G. S., Holmström, M., Barabash, S., Futaana, Y., . . . Wieser, M. (2021). Solar cycle variation of ion escape from mars. *Icarus*, 114610. doi: 10.1002/grl.50149

Pollack, J. B., Kasting, J. F., Richardson, S. M., & Poliakoff, K. (1987). The case for a wet, warm climate on early mars. *Icarus*, *71*(2), 203–224.

Ramstad, R., & Barabash, S. (2021). Do intrinsic magnetic fields protect planetary atmospheres from stellar winds? *Space Science Reviews*, *217*(2), 1-39.

Ramstad, R., Barabash, S., Futaana, Y., Nilsson, H., & Holmström, M. (2018). Ion escape from mars through time: An extrapolation of atmospheric loss based on 10 years of mars express measurements. *Journal of Geophysical Research: Planets*, *123*, 3051–3060. doi: 10.1029/2018JE005727

Ramstad, R., Barabash, S., Futaana, Y., Nilsson, H., Wang, X.-D., & Holmström, M. (2015). The martian atmospheric ion escape rate dependence on solar wind and solar euv conditions: 1. seven years of mars express observations. *Journal of Geophysical Research: Planets*, *120*(7), 1298–1309.

Schunk, R. W., & Nagy, A. F. (2009). *Ionospheres.* New York: Cambridge University Press.

Thiemann, E. M., Chamberlin, P. C., Eparvier, F. G., Templeman, B., Woods, T. N., Bougher, S. W., & Jakosky, B. M. (2017). The maven euvm model of solar spectral irradiance variability at mars: Algorithms and results. *Journal of Geophysical Research: Space Physics*, *122*(3), 2748–2767.

Weber, T., Brain, D., Xu, S., Mitchell, D., Espley, J., Mazelle, C., . . . Jakosky, B. (2021). Martian crustal field influence on o+ and o2+ escape as measured by maven. *Journal of Geophysical Research: Space Physics*, *126*(8), e2021JA029234.

Supporting Information for "Solar and solar wind energy drivers for O^+, and O_2^+ ion escape at Mars"

N. R. Schnepf[1], Y. Dong[1], D. Brain[1], K. G. Hanley[3], W. K. Peterson[1], R. J. Strangeway[2], E. M. B. Thiemann[1], J. S. Halekas[4], J. R. Espley[5], F. Eparvier[1], J. P. McFadden[3]

[1]Laboratory for Atmospheric and Space Physics, University of Colorado Boulder, Boulder, CO, USA

[2]Institute of Geophysics and Planetary Physics, and Department of Earth, Planetary, and Space, University of California Los Angeles, Los Angeles, CA, USA

[3]Space Sciences Laboratory, University of California Berkeley, Berkeley, CA, USA

[4]Department of Physics and Astronomy, University of Iowa, Iowa City, IA, USA

[5]NASA Goddard Space Flight Center, Greenbelt, MD, USA

Contents of this file

Corresponding author: Neesha R. Schnepf, Laboratory for Atmospheric and Space Physics, University of Colorado Boulder, 3665 Discovery Dr, Boulder, CO 80303, USA. (neesha.schnepf@lasp.colorado.edu)

Data density for solar wind kinetic energy flux bins:

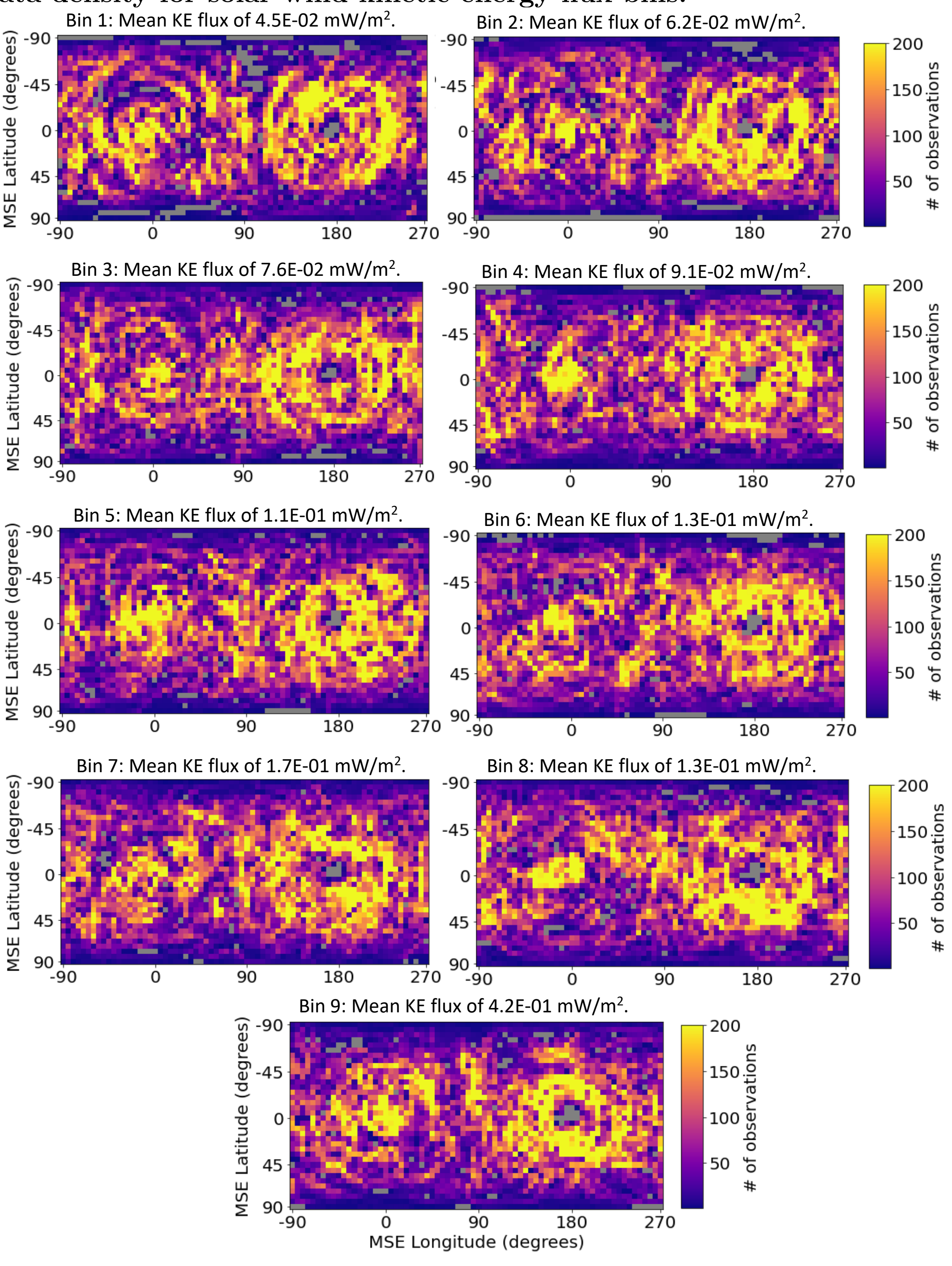

S1. The density of ion flux observations in each grid cell is shown for each solar wind kinetic energy flux bin.

Data density for solar wind electromagnetic energy flux bins:

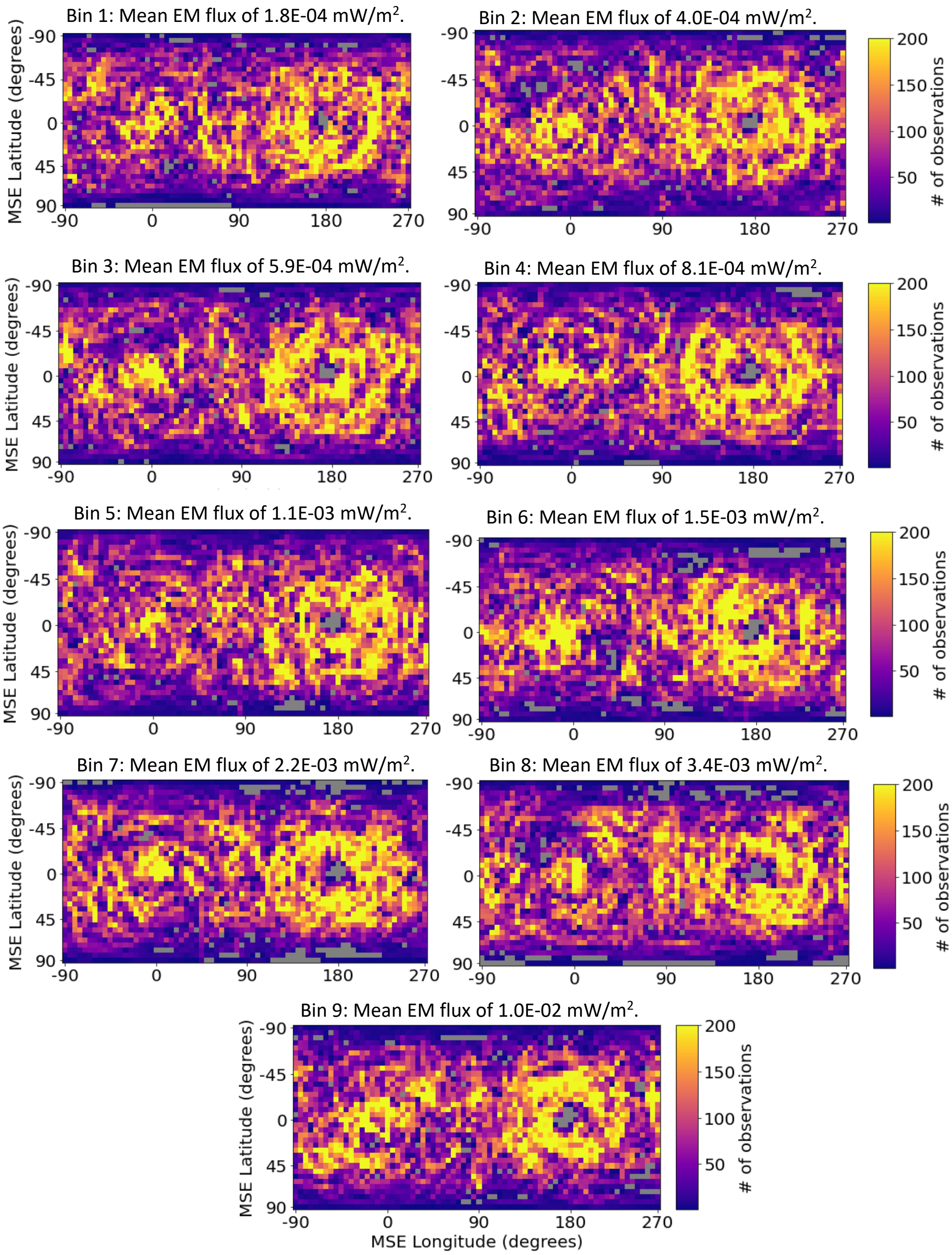

S2. The density of ion flux observations in each grid cell is shown for each solar wind electromagnetic energy flux bin.

Data density for total solar irradiance bins:

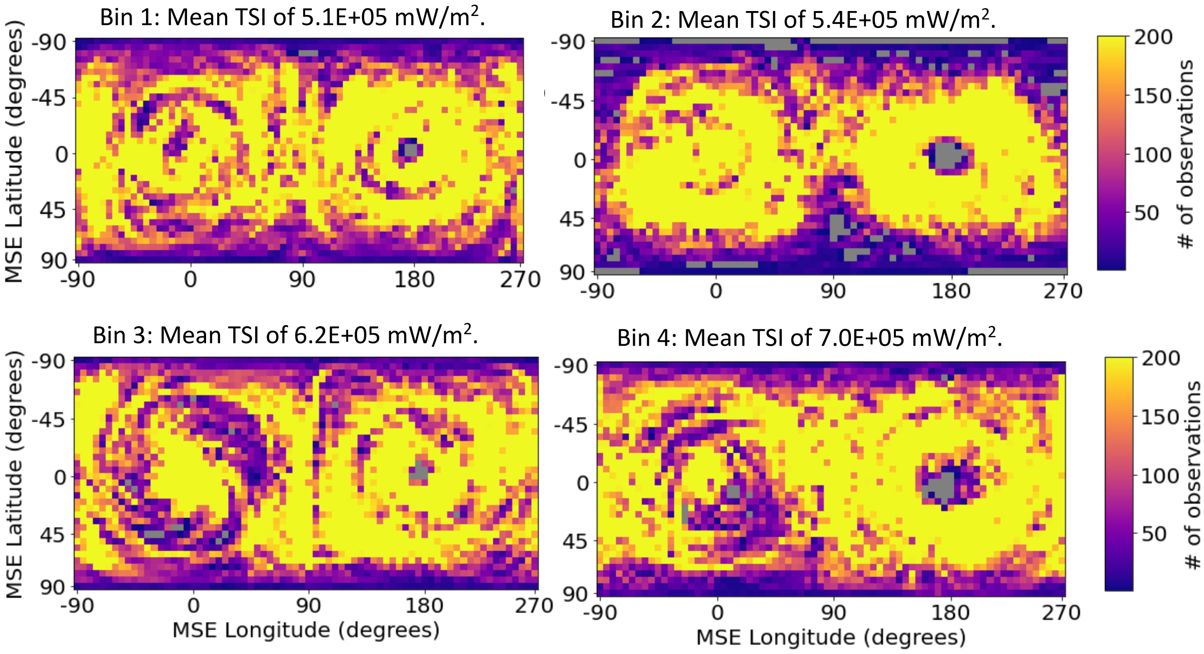

S3. The density of ion flux observations in each grid cell is shown for each total solar irradiance bin.

Data density for solar ionizing irradiance bins:

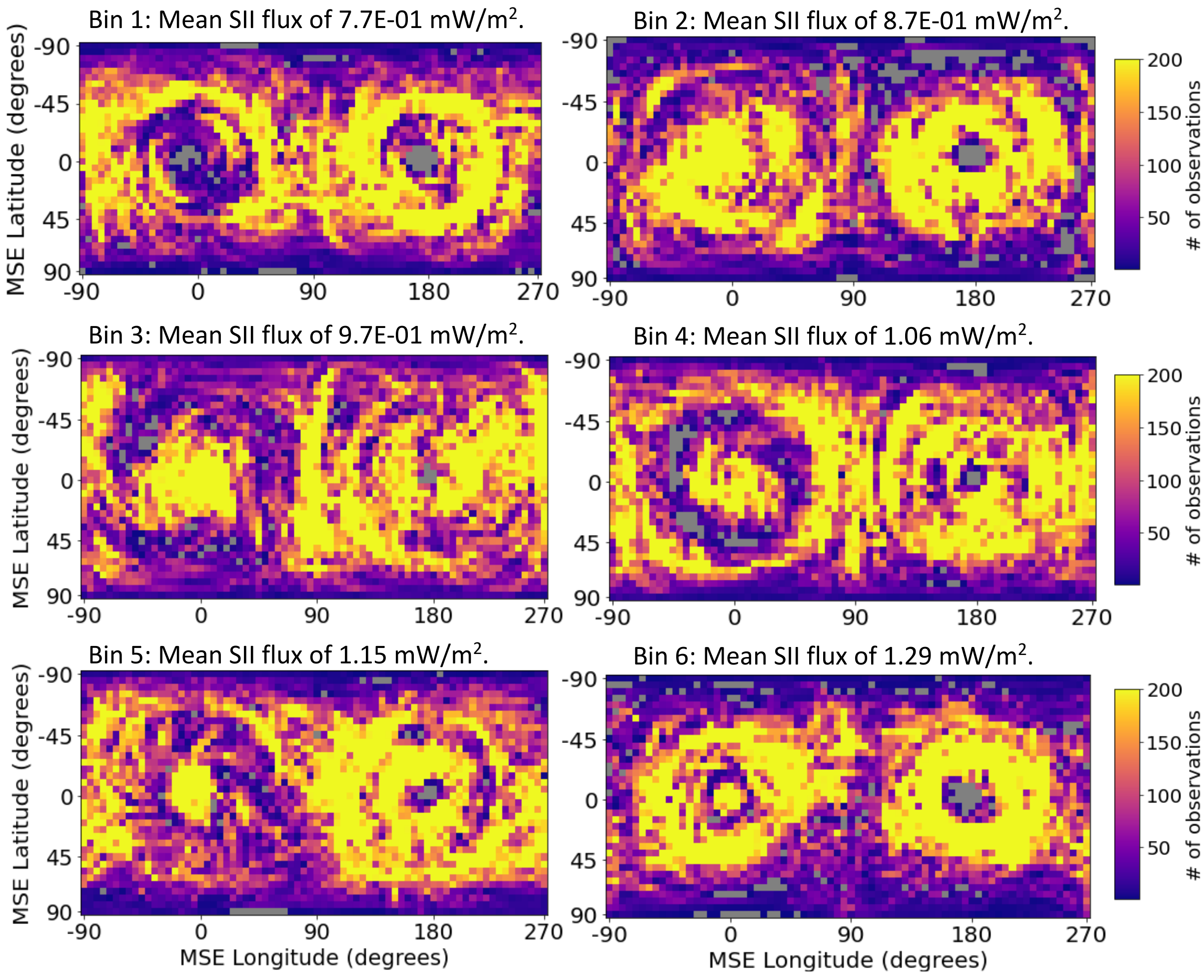

S4. The density of ion flux observations in each grid cell is shown for each solar ionizing irradiance bin.

Ion flux maps for the solar wind kinetic energy bins, O^+:

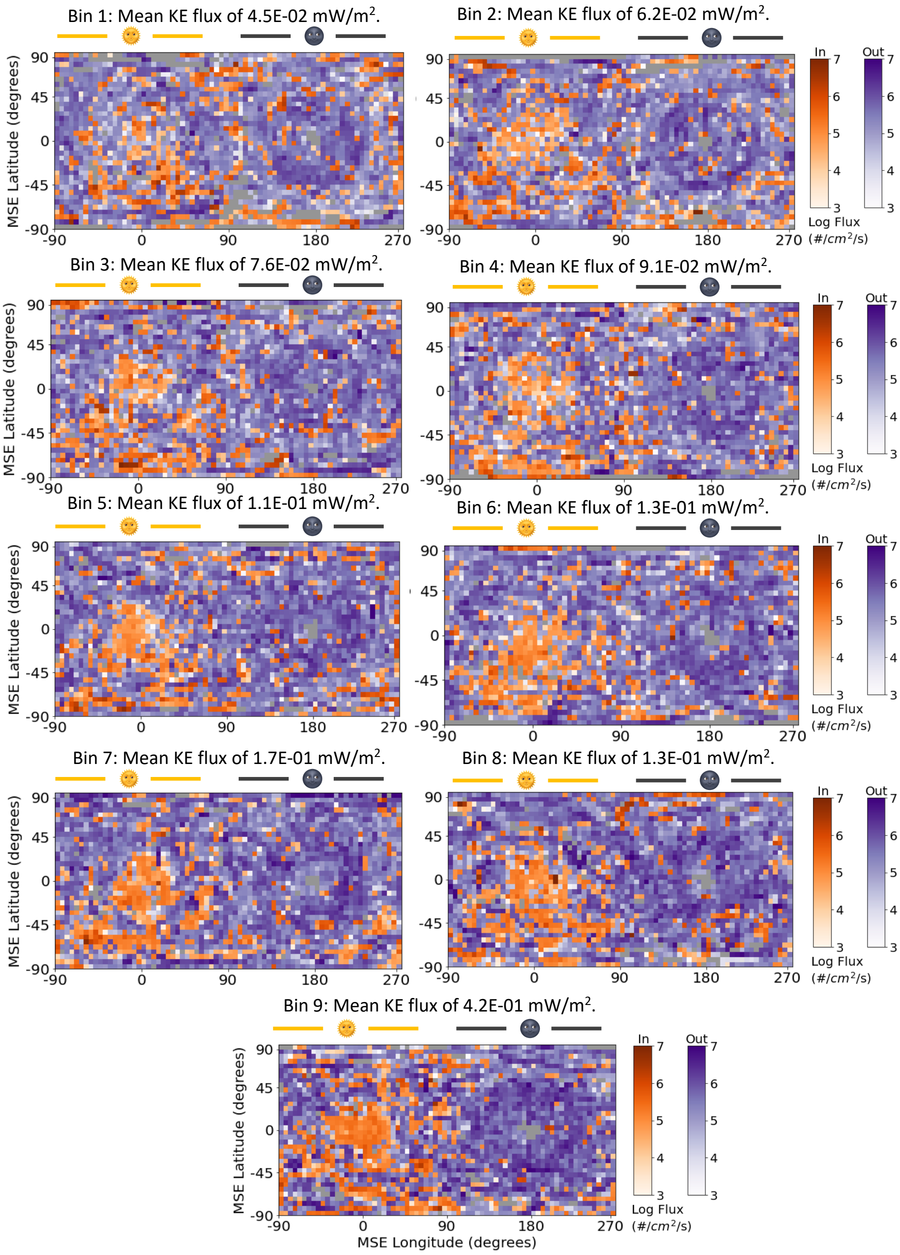

S5b. The average observed outwards (purple) and inwards (orange) net flux for O^+ from February 1, 2016 to May 21, 2022 for the solar wind kinetic energy flux bins. The data is on a Mars Solar Electric grid; the day-side and night-side of Mars are denoted accordingly.

Ion flux maps for the solar wind kinetic energy bins, O_2^+:

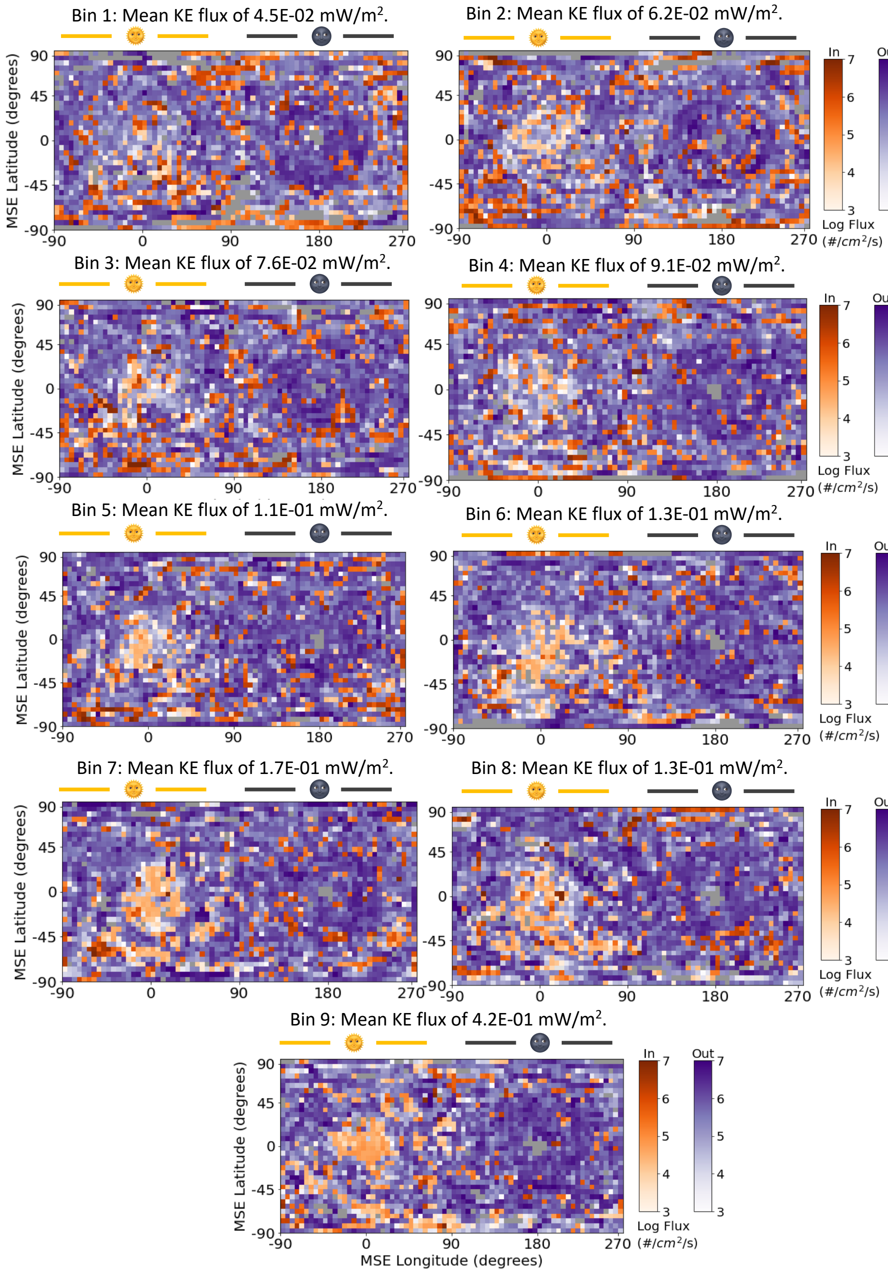

S5c. The average observed outwards (purple) and inwards (orange) net flux for O_2^+ from February 1, 2016 to May 21, 2022 for the solar wind kinetic energy flux bins. The data is on a Mars Solar Electric grid; the day-side and night-side of Mars are denoted accordingly.

Ion flux maps for the solar wind electromagnetic energy bins, O^+:

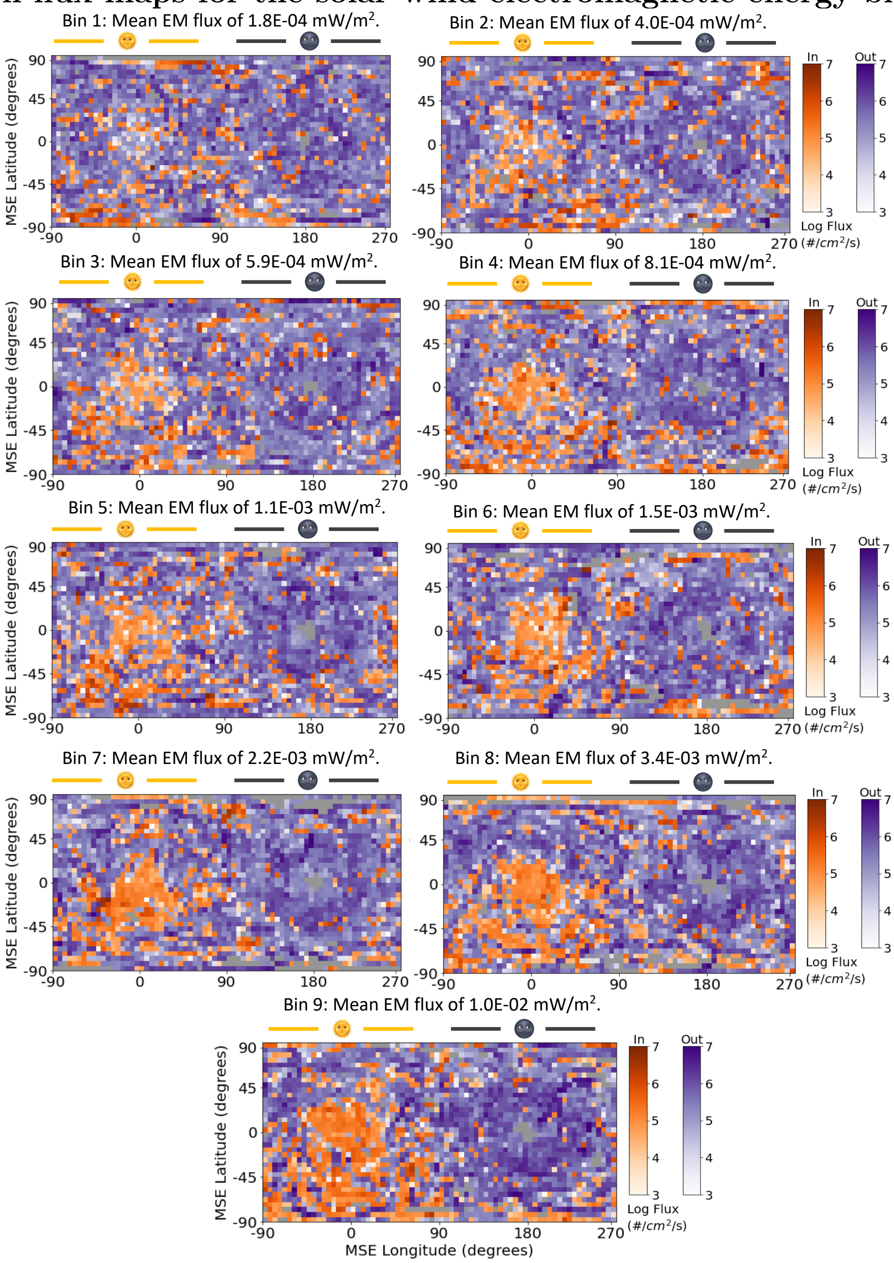

S6b. The average observed outwards (purple) and inwards (orange) net flux for O^+ from February 1, 2016 to May 21, 2022 for the solar wind electromagnetic energy flux bins. The data is on a Mars Solar Electric grid; the day-side and night-side of Mars are denoted accordingly.

Ion flux maps for the solar wind electromagnetic energy bins, O_2^+:

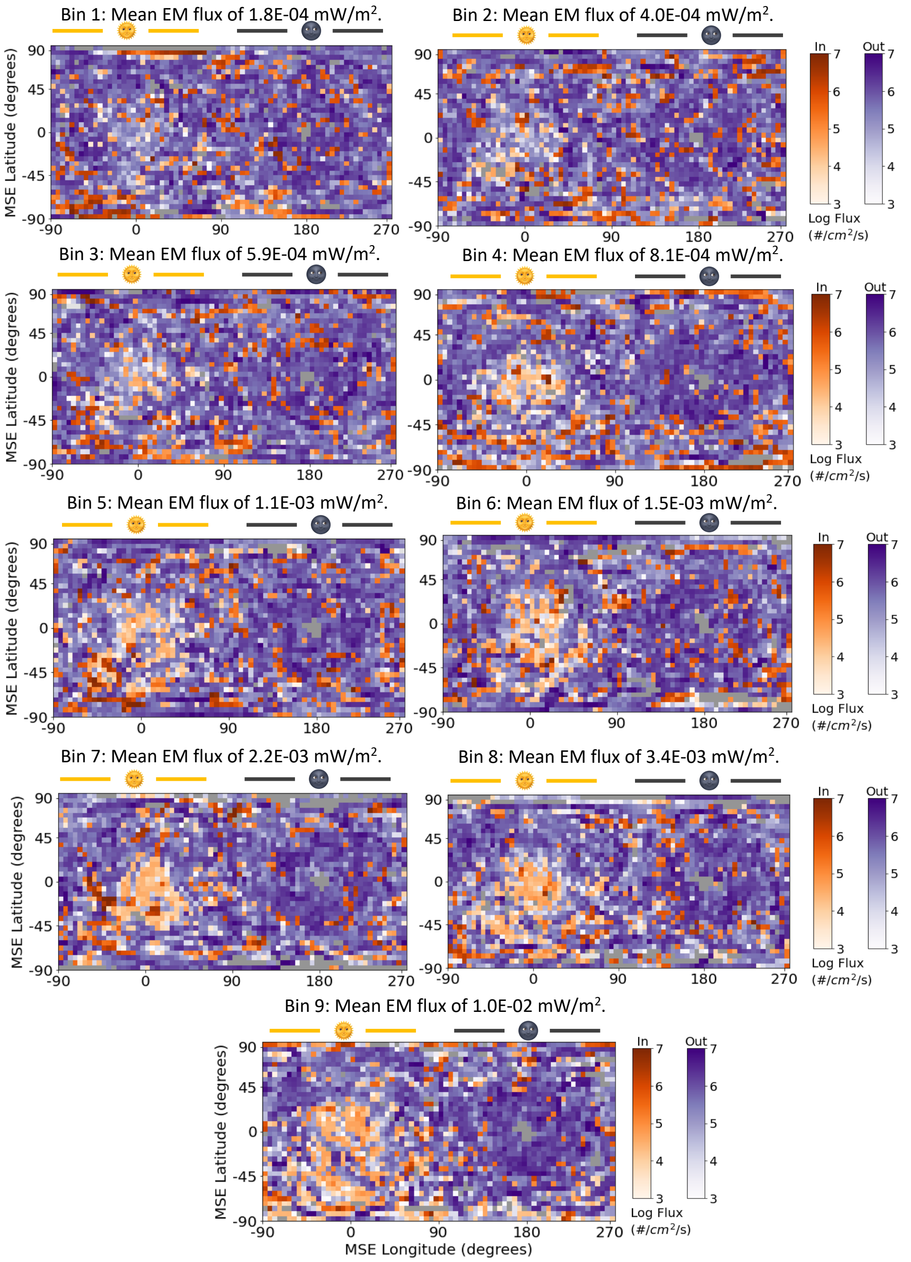

S6c. The average observed outwards (purple) and inwards (orange) net flux for O_2^+ from February 1, 2016 to May 21, 2022 for the solar wind electromagnetic energy flux bins. The data is on a Mars Solar Electric grid; the day-side and night-side of Mars are denoted accordingly.

Ion flux maps for the solar ionizing irradiance bins, O^+:

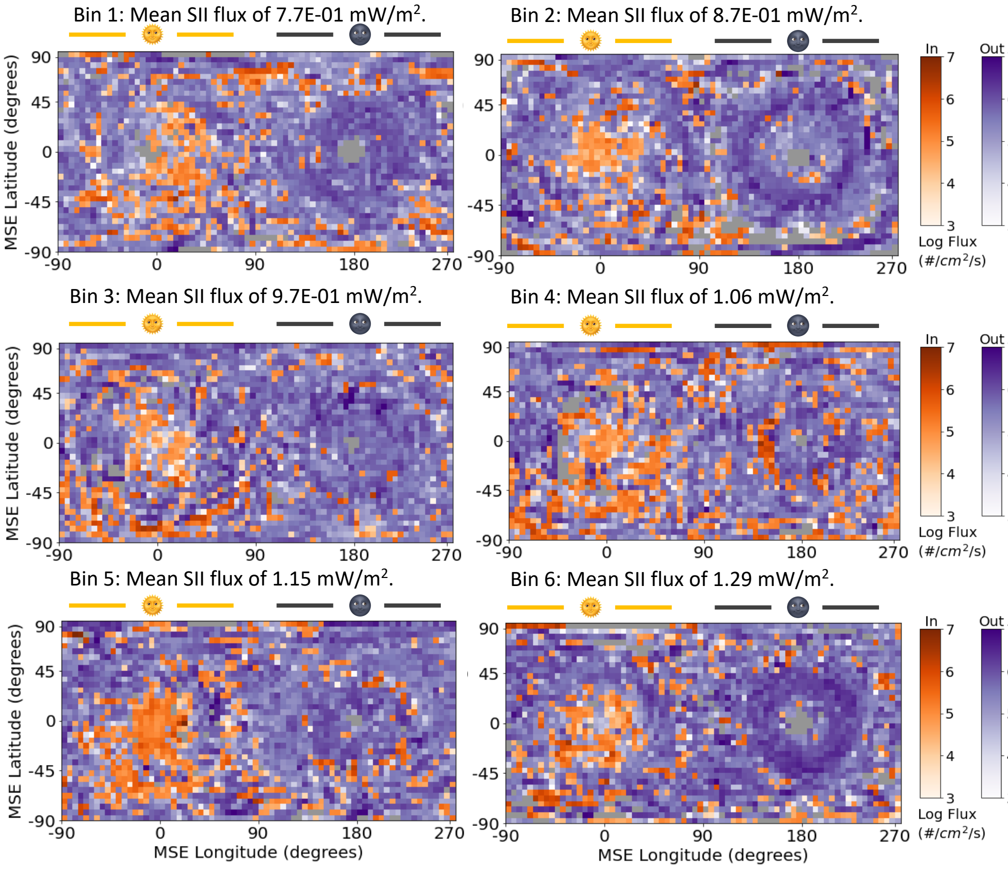

S7b. The average observed outwards (purple) and inwards (orange) net flux for O^+) from February 1, 2016 to May 21, 2022 for the solar ionizing irradiance bins. The data is on a Mars Solar Electric grid; the day-side and night-side of Mars are denoted accordingly.

Ion flux maps for the solar ionizing irradiance bins, O_2^+:

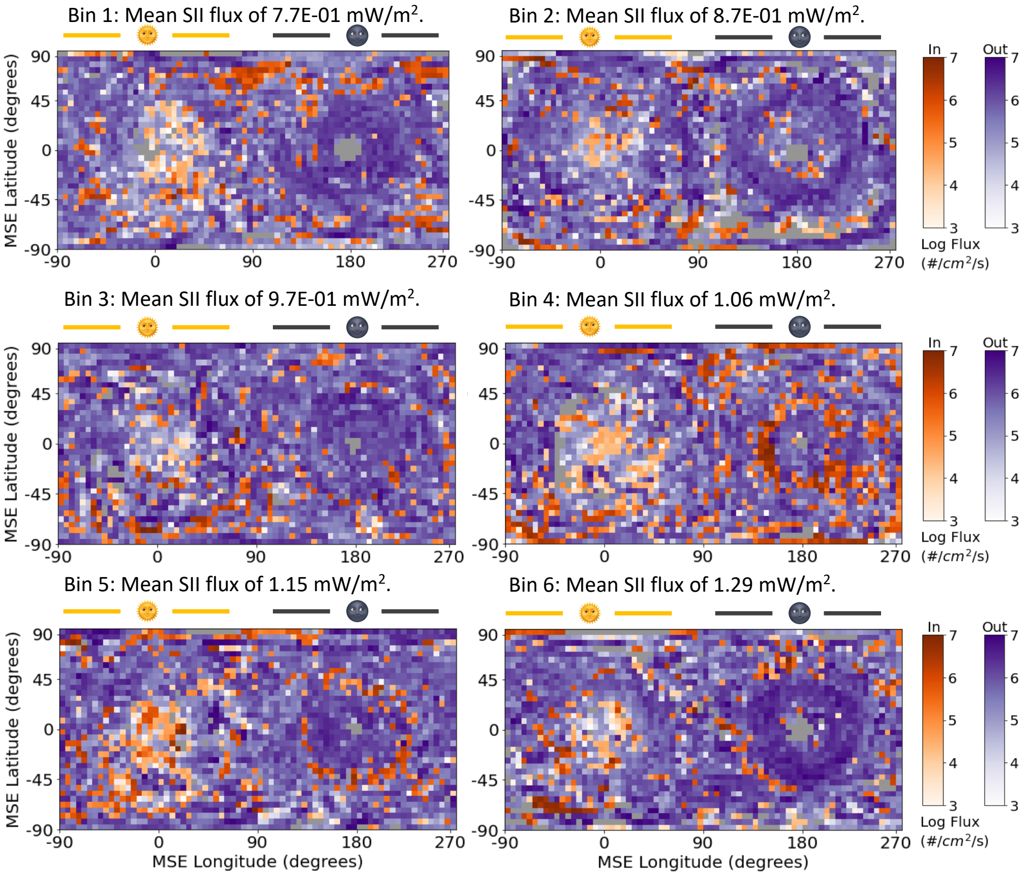

S7c. The average observed outwards (purple) and inwards (orange) net flux for O_2^+) from February 1, 2016 to May 21, 2022 for the solar ionizing irradiance bins. The data is on a Mars Solar Electric grid; the day-side and night-side of Mars are denoted accordingly.

Ion flux maps for the total solar irradiance, O^+:

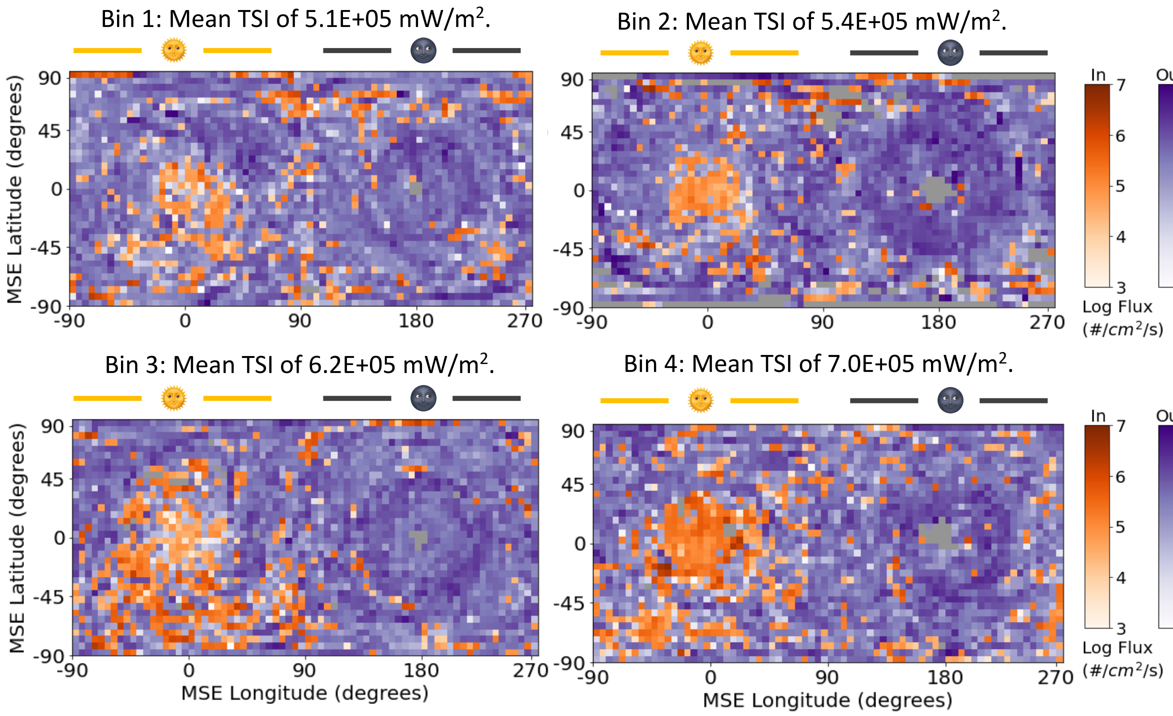

S8b. The average observed outwards (purple) and inwards (orange) net flux for O^+ from February 1, 2016 to May 21, 2022 for the total solar irradiance bins. The data is on a Mars Solar Electric grid; the day-side and night-side of Mars are denoted accordingly.

Ion flux maps for the total solar irradiance, O_2^+:

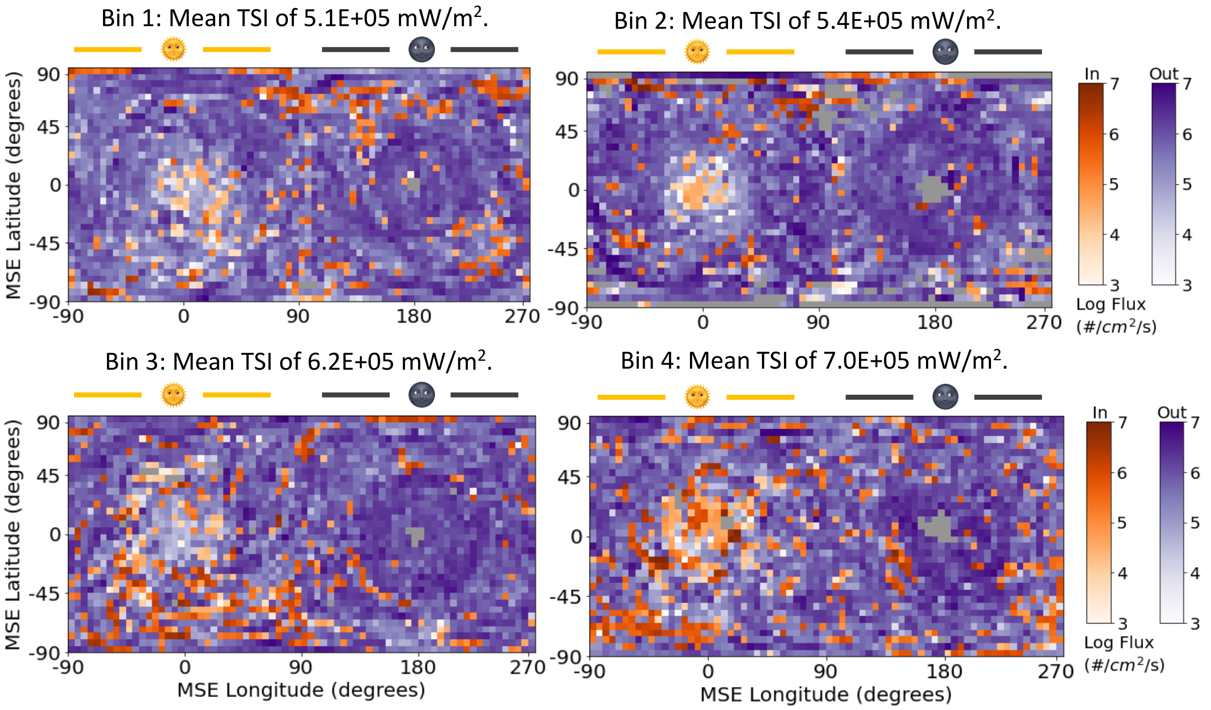

S8c. The average observed outwards (purple) and inwards (orange) net flux for O_2^+ from February 1, 2016 to May 21, 2022 for the total solar irradiance bins. The data is on a Mars Solar Electric grid; the day-side and night-side of Mars are denoted accordingly.

Solar wind kinetic energy flux versus solar wind electromagnetic energy flux:

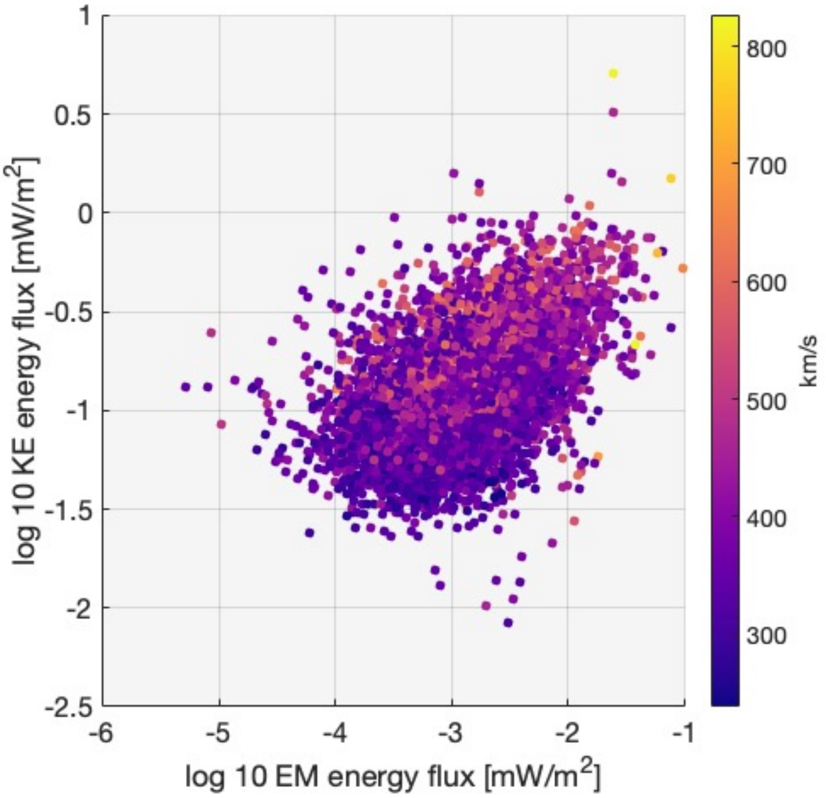

S9. Solar wind kinetic energy flux versus solar wind electromagnetic energy flux with observations color coded by solar wind proton velocity. These solar wind energy fluxes are mutually correlated. Accounting for this was beyond the scope of our study, but should be considered in future work seeking to empirically fit for either driver.

Solar wind electromagnetic energy flux versus total solar irradiance:

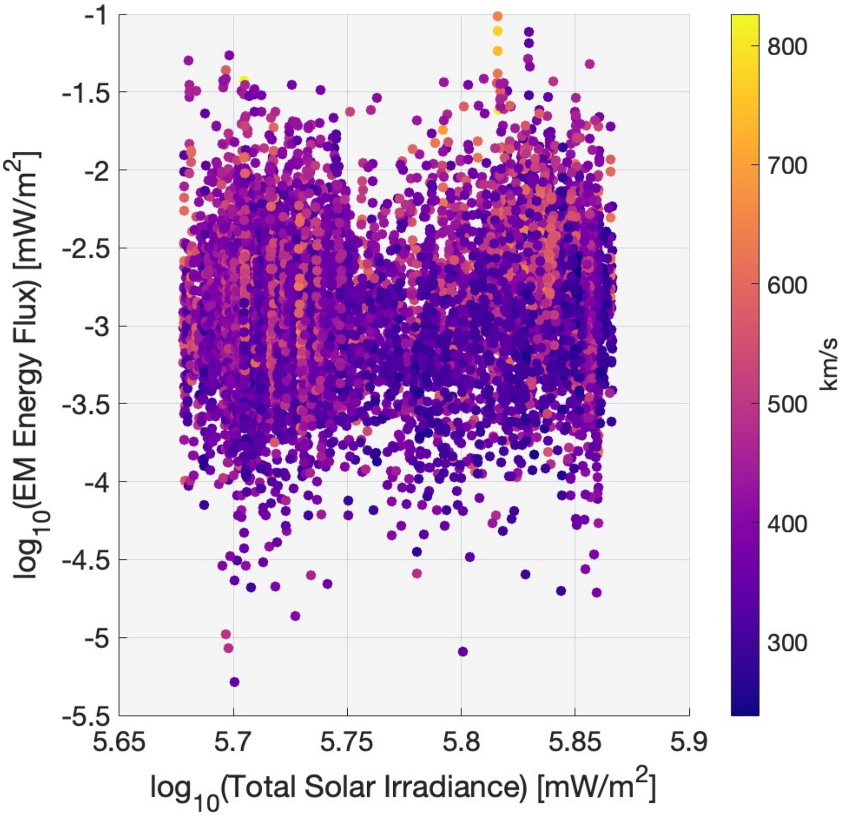

S10. Solar wind electromagnetic energy flux versus total solar irradiance with observations color coded by solar wind proton velocity. There is no obvious correlation between solar wind electromagnetic energy flux and total solar irradiance.

Solar wind electromagnetic energy flux versus solar ionizing irradiance:

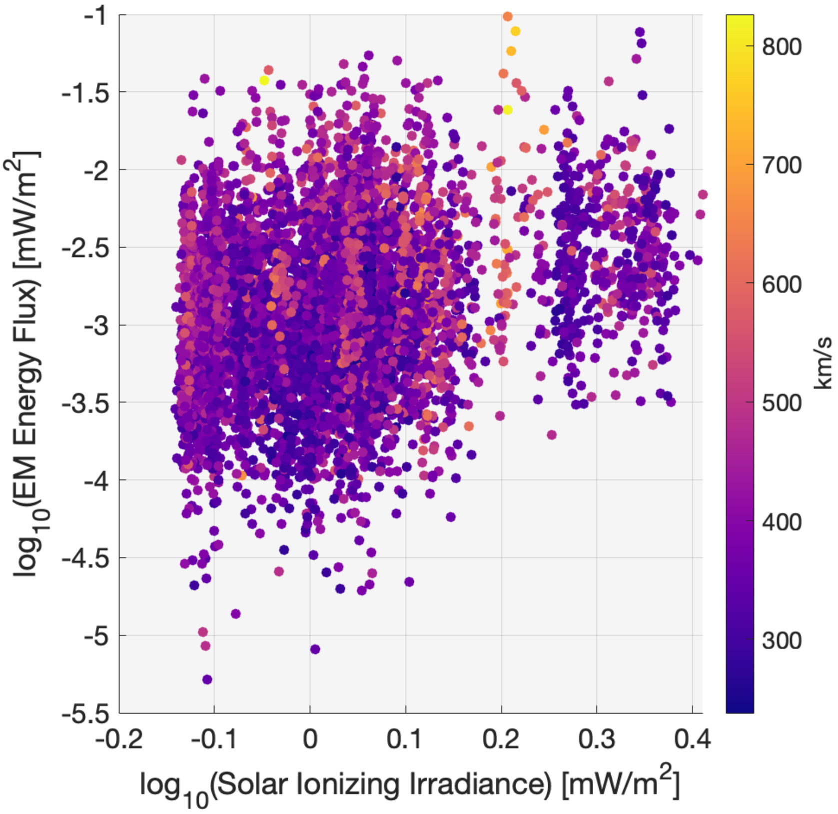

S11. Solar wind electromagnetic energy flux versus solar ionizing irradiance with observations color coded by solar wind proton velocity. There is no obvious correlation between solar wind electromagnetic energy flux and solar ionizing irradiance, although there certainly are more solar wind observations for smaller values of solar ionizing irradiance. Using Mars mission data during solar maximum could better fill observations for higher solar ionizing irradiances.

Solar wind kinetic energy flux versus total solar irradiance:

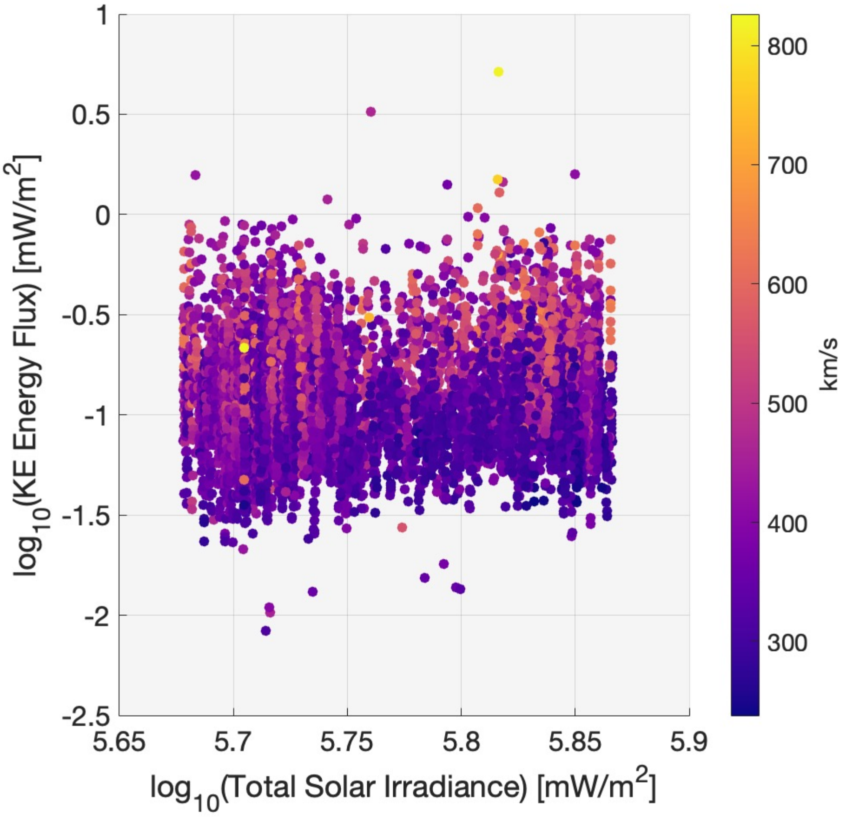

S12. Solar wind kinetic energy flux versus total solar irradiance with observations color coded by solar wind proton velocity. There is no obvious correlation between solar wind kinetic energy flux and total solar irradiance.

Solar wind kinetic energy flux versus solar ionizing irradiance:

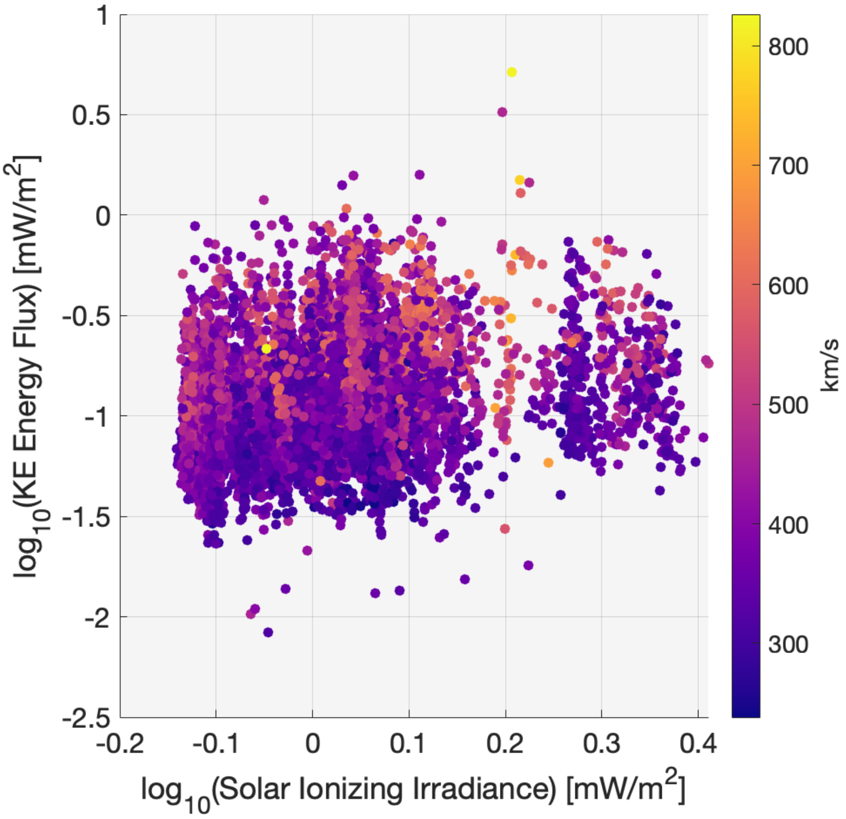

S13. Solar wind kinetic energy flux versus solar ionizing irradiance with observations color coded by solar wind proton velocity. There is no obvious correlation between solar wind kinetic energy flux and solar ionizing irradiance, although there certainly are more solar wind observations for smaller values of solar ionizing irradiance. Using Mars mission data during solar maximum could better fill observations for higher solar ionizing irradiances.

Solar ionizing irradiance versus total solar irradiance:

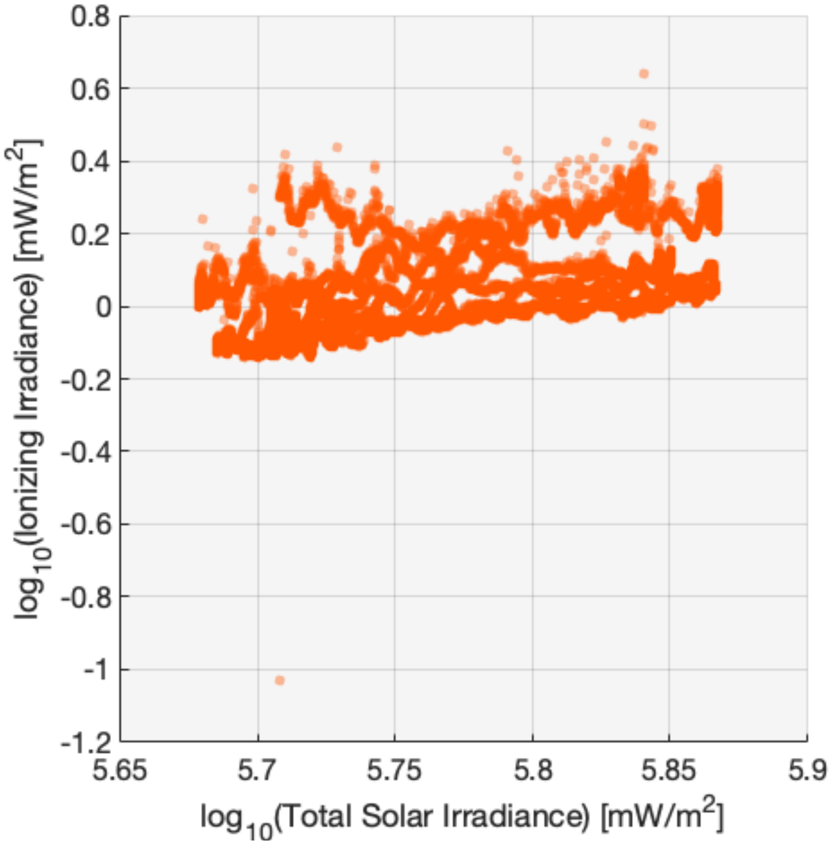

S14. Solar ionizing irradiance versus total solar irradiance. There is mutual correlation between these solar irradiances.